RADAR

Research Archive and Digital Asset Repository

This version is available: https://radar.brookes.ac.uk/radar/items/42b2cc5e-5758-4ec5-b15a-701fb81f43fb/1/

WWW.BROOKES.AC.UK/GO/RADAR

Characterizing the cavitation development and acoustic spectrum in various liquids

I. Tzanakis [a,b,*], G.S.B. Lebon [c], D.G. Eskin [a,d], K.A. Pericleous [c]

[a] Brunel University London, Brunel Centre for Advanced Solidification Technology (BCAST), Uxbridge, London UB8 3PH, United Kingdom
[b] Oxford Brookes University, Faculty of Technology, Design and Environment, Oxford OX33 1HX, United Kingdom
[c] University of Greenwich, Computational Science and Engineering Group, London SE10 9LS, United Kingdom
[d] Tomsk State University, Smart Materials and Technologies Institute (SMTI), Tomsk 634050, Russia

ARTICLE INFO

ABSTRACT

A bespoke cavitometer that measures acoustic spectrum and is capable of operating in a range of temperatures (up to 750 °C) was used to study the cavitation behaviour in three transparent liquids and in molten aluminium. To relate these acoustic measurements to cavitation development, the dynamics of the cavitation bubble structures was observed in three Newtonian, optically transparent liquids with significantly different physical properties: water, ethanol, and glycerine. Each liquid was treated at 20 kHz with a piezoelectric ultrasonic transducer coupled to a titanium sonotrode with a tip diameter of 40 mm. Two different transducer power levels were deployed: 50% and 100%, with the maximum power corresponding to a peak-to-peak amplitude of 17 μm. The cavitation structures and the flow patterns were filmed with a digital camera. To investigate the effect of distance from the ultrasound source on the cavitation intensity, acoustic emissions were measured with the cavitometer at two points: below the sonotrode and near the edge of the experimental vessel. The behaviour of the three tested liquids was very different, implying that their physical parameters played a decisive role in the establishment of the cavitation regime. Non dimensional analysis revealed that water shares the closest cavitation behaviour with liquid aluminium and can therefore be used as its physical analogue in cavitation studies; this similarity was also confirmed when comparing the measured acoustic spectra of water and liquid aluminium.

1. Introduction

Acoustic cavitation involves the formation, growth, pulsation, and collapse of micro-bubbles in liquids under high-intensity ultrasound waves. Cavitation is initiated when the amplitude of the acoustic pressure exceeds a threshold e.g. ∼0.15 MPa for liquid glycerine [1], 0.06–0.1 MPa for distilled water [2], and ∼0.7 MPa for molten aluminium [2] for driving frequencies around 20 kHz. With further increase in acoustic pressure, there is a transition to the developed cavitation regime where thousands of micro-bubbles are formed. These bubbles expand during the rarefaction phase and rapidly collapse during the compression phase of ultrasound, thereby producing high-speed jets (300–1000 m/s) and local hydrodynamic impact pressures in the range of GPa [3]. These phenomena are believed to be responsible for mixing,

fragmentation, erosion, wetting, sono-capillary, and other effects that have various practical industrial applications [2–4].

Multi-bubble systems have been vigorously studied in recent years. However, the dramatic fluctuations of bubble ensembles, the complex interactions between bubbly clouds, and their non-linear cavitation activity make it difficult to observe and model cavitation in a consistent and thorough manner [5]. Nevertheless, with suitable cavitation detectors [6,7], broadband acoustic emissions from micro-bubbles undergoing acoustic cavitation can be detected. High-order resolution of the frequency spectrum allows the determination, characterization, and quantification of the cavitation regime with great accuracy.

Key features of a typical acoustic spectra include:
(i) sharp peaks corresponding to harmonics and ultra-harmonics of the acoustic driving frequency with further contributions from the non-linear dynamics of cavitation bubbles;
(ii) sub-harmonics related to the excitation of bubbles at sub-harmonic resonances that indicates the inception of cavitation regime [8]; and

---

(iii) a continuous broadband component, commonly known as "white noise" or "cavitation noise", which is linked to the occurrence of violent inertial cavitation at large acoustic intensities [9].

The choice of the driving frequency, and consequently the size range of cavitating bubbles, is very important for both physical and chemical effects. Specifically, it is shown that driving frequencies in the low frequency range (i.e. 20 kHz) are associated with larger and violently collapsing bubbles that are mostly responsible for mechanical effects such as surface deformation, erosion, de-agglomeration, and fragmentation while driving frequencies in the MHz range are associated with a shorter life cycle of smaller cavitation bubbles that affect chemical reactions and cleaning [10]. The frequency spectrum analysis provides substantial information on the characteristics of cavitation in a liquid volume. By analysing the prominent peaks across the frequency spectrum as has been done in Refs. [11,12], regions of higher cavitation activity can be revealed and the mean size of active cavitation bubbles can be estimated.

In this work, we examined the effects of liquid properties on the development of the cavitation zone, the behaviour of the cavitation cloud, and the corresponding acoustic emissions. To identify the characteristic frequencies due to cavitation development at two acoustic powers, a detailed analysis of three liquid environments with distinctly different properties – water, ethanol, and glycerine – was conducted by observing the cavitation structures and analysing the frequency spectra received by a bespoke cavitometer capable of working in a range of temperatures [6]. Active cavitation bubbles and bubble cloud formation were observed macroscopically using a high definition digital camera. The magnitudes of broadband cavitation noise of the tested liquids were compared. To the authors' knowledge, this is the first attempt of systematic characterization and comparison of cavitation development in these three liquids. The results were analysed with dimensionless parameters, and the acoustic spectra for water and liquid aluminium were compared. The results of this study may be useful for the selection of a transparent analogue for opaque liquids such as molten aluminium, which are now in the focus of technological development of ultrasonic processing [2,4,11,12].

2. Methods and materials

2.1. Experimental setup

A 1-kW piezoelectric transducer (Hielscher UIP1000HD) operating at 20 kHz induced ultrasonic oscillations continuously in three transparent liquids, i.e. de-ionised water, ethanol and glycerine, via a cylindrical titanium sonotrode of 40-mm diameter. These three liquids were not degassed prior to the experiments. The tested liquid was contained in a rectangular, glass-walled tank with the base area 290 mm × 210 mm. The liquid height was 110 mm. The radiating surface of the vertically mounted sonotrode was immersed 20 mm below the liquid surface. There is a limited choice of variables that can be kept constant in the experiment: one is the frequency (20 kHz), another is either the input power or the oscillation amplitude. In this work, we have selected to keep the amplitude constant for comparison of different liquids (albeit we performed two series of comparison at two levels of constant amplitude). The amplitude of the vibrating surface was 17 μm peak-to-peak in all liquids when the sonotrode operated at 100% power (and 8.5 μm peak-to-peak at 50%). The acoustic power at the tip of the sonotrode was monitored by subtracting the input electric power of the transducer when sonotrode operates in the studied liquid from that measured in the reference medium (air). This value was recorded using a wattmeter integrated to the transducer device. The acoustic powers of the sonotrode were 90 ± 3 W, 78 ± 2 W and 230 ± 5 W for water, ethanol, and glycerine, respectively, when operating at 100% power. The temperature was continuously monitored during the experiments and was maintained at 21 ± 1 °C.

The cavitation and flow patterns were recorded using a high definition digital camera at 30 frames per second. Each experiment was repeated at least five times with very good reproducibility of the observed effects.

The cavitometer probe [6] with a spatial resolution of about 50 mm and a bandwidth of up to 10 MHz captured the acoustic spectra. Measurements of the acoustic emissions with this probe were performed at two points as shown in Fig. 1: i) below the sonotrode and ii) near the edge of the tank (110 ± 2 mm off the sonotrode axis).

The cavitometer consists of a 4 mm diameter tungsten waveguide that can be submerged into the liquid up to a depth of 100 mm; at the other end, the waveguide is connected to a piezo-electric sensor that converts the mechanical vibrations into an electrical signal. This signal is acquired by the measuring device after amplification. The waveguide of the cavitometer probe was submerged 40 ± 2 mm below the liquid free surface. The probe calibration has been performed in collaboration with the National Physical Laboratory (Teddington, UK) using independently calibrated vessels, sources, and hydrophones. A full account of the cavitometer design and performance can be found elsewhere [6].

Finally, cavitation emissions in liquid aluminium and water were compared. For this comparison, both liquids were sonicated
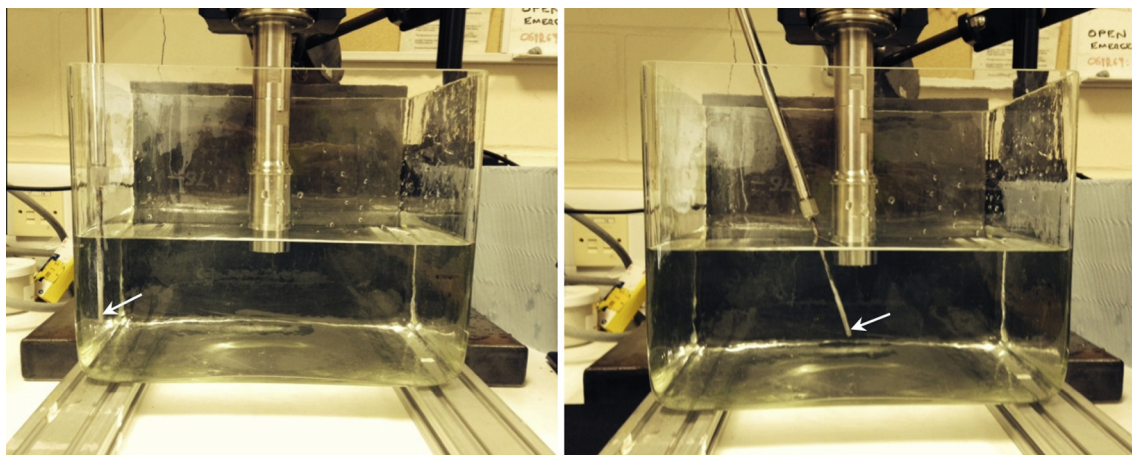

Fig. 1. Experimental test rig: a cavitometer (tip is shown by the arrow) placed a) nearby the edge of the vessel and b) below the sonotrode.

by a water-cooled 5-kW magnetostrictive transducer (Reltec) coupled with a cylindrical niobium tip submerged 20 mm below the free surface. The input power of the generator was adjusted to 3.5 kW, with the driving frequency maintained at 17.5 kHz. The use of a magnetostrictive transducer was necessary as the piezoelectric transducer used for room-temperature experiments cannot be used at the high temperatures of molten aluminium [2]. The sonicated liquid was contained in a cylindrical vessel of diameter 150 mm. The liquid height in the vessel was 110 mm (approximately 2000 cm^3). The temperature of water was maintained at 22 ± 2 °C and while that of molten aluminium was maintained at 710 ± 10 °C. There was no controlled atmosphere. A detailed description of the experimental test rig can be found elsewhere [13].

2.2. Data acquisition

An external digital oscilloscope (Picoscope series 2204) that was attached to the cavitometer acquired the frequency spectra. Picoscope allowed real-time signal monitoring of the cavitometer sensor's data and ultrasonic parameters. A Blackman window was applied to the raw voltage signal, which was then transformed to the frequency domain via a Fast Fourier Transform (FFT). The data were acquired when a steady state condition was achieved: the minimum voltage of each data set from the sensor was averaged and monitored. The data were captured when there was no change in the average value of the minimum voltage. The acquired spectrum was the average of 30 measurements, each corresponding to the FFT of a 1 ms signal with resolution of 0.762 kHz. To ensure reproducibility of results, each measurement was repeated three times.

2.3. Liquid properties

The properties of the three different liquids – water, glycerine and ethanol – together with those of liquid aluminium at 700 °C are shown in Table 1. Pure aluminium was selected as a material for comparison because it is extensively studied and widely used in metallurgical, automotive, and aerospace industry as an alloy base.

2.4. Acoustic spectrum analysis

Spectra measurements with the cavitometer probe revealed the presence of discrete harmonics (nf_0) generated at integer frequencies (n) of the fundamental driving frequency (f_0), half-order subharmonic ($f_0/2$), ultra-harmonics ($nf_0/2$, $nf_0/4$), and the broadband component at MHz frequencies. The broadband noise is mainly associated with transient (inertial) cavitation and originates from various events: temporally symmetrical, usually small radius bubbles; asymmetrical, usually larger radius bubbles; fluctuations of cavitation bubbles; the non-periodic pulsation of bubbles, as well as their shock wave emissions during collapse or implosion [15]. Furthermore, satellite bubbles merging and collapsing into small clouds may also contribute to the broadband noise [16]. In contrast, sharp distinctive peaks in the low frequency domain (kHz) as well as consistent periodic peak patterns in the high frequency domain (MHz) are associated with linearly and nonlinearly oscillating stable (non-inertial) cavitation bubbles, with significant lifecycles giving rise to acoustic spectra at particular frequencies [9]. Thus, the spectrum of acoustic cavitation noise is a combination of the acoustic emissions from cavitating bubbles of various sizes [17]. For example, at a 20 kHz driving frequency in water, a fairly large pulsating bubble, i.e. 150–200 µm in diameter, gives rise to sharp distinctive peaks in the low-frequency spectrum domain. If this bubble collapses and produces a swarm of small satellite bubbles, the new associated frequencies result in a multi-peak acoustic signal and the shock waves from the collapse contribute to the broadband noise.

3. Results and discussion

3.1. Observations of the cavitation zone

Fig. 2 demonstrates the main differences in bubble cloud structures in each liquid. In water, the stable conical bubble structure that has been reported in the literature, e.g. [18], is formed (Fig. 2a). In glycerine, only a few experimental studies regarding the development of the cavitation zone have been conducted [19–21]. In these studies, only limited information on cavitation development was given and no generalization was provided. In the current study, it is shown that a thick round layer delimits the borders of the cavitation zone in glycerine and bubble transport due to acoustic streaming develops sluggishly over time (Fig. 2b). To the authors' best knowledge, there were no previous reports on the acoustic cavitation, development of the cavitation zone and bubble dynamics behaviour in ethanol apart from the work of Plesset [22] where cavitation damage rate in liquid ethanol was considered and some qualitative differences in the cavitation bubble cloud were shown. In this study, we observed fairly large cavitation bubbles (easily distinguished by naked eye, see Fig. 2c) that are mainly dispersed and have a tendency to vigorously oscillate moving towards the free surface (see Fig. 2c, dashed arrow) rather than creating complicated bubbly structures and generating multiple collapsing events. In the following sections we will discuss these observations in more detail.

3.1.1. De-ionised water

In de-ionised water, typical conical bubble structures were clearly observed only at the maximum sonotrode amplitude (17 µm p-p). At 50% (8.5 µm p-p) acoustic power, the bubbly streamers were not yet stable and randomly fluctuate in space.

Table 1
Material properties for water, glycerine, ethanol, and molten aluminium [2,14]. Surface tension with air interface for water, glycerine, and ethanol; hydrogen interface for aluminium.

|	Water	Glycerine	Ethanol	Aluminium
Temperature (°C)	20	20	20	700
Density ρ (kg m^{-3})	1000	1260	785	2375
Dynamic viscosity μ (Pa s)	1.0×10^{-3}	0.95	1.1×10^{-3}	1.3×10^{-3}
Kinematic viscosity ν (m^2 s^{-1})	1.0×10^{-6}	7.5×10^{-4}	1.4×10^{-6}	5.5×10^{-7}
Speed of sound c (m s^{-1})	1482	2000	1100	4600
Surface tension σ (N m^{-1})	0.079	0.064	0.022	0.86
Vapour pressure p_v (Pa)	2.2×10^3	Negligible	5.3×10^3	Negligible
Thermal conductivity κ (W m^{-1} K^{-1})	0.58	0.285	0.014	250
Specific heat c_p (J kg^{-1} K^{-1})	4183	2430	2400	910
Volume expansivity α (K^{-1})	207×10^{-6}	500×10^{-6}	1090×10^{-6}	69×10^{-6}
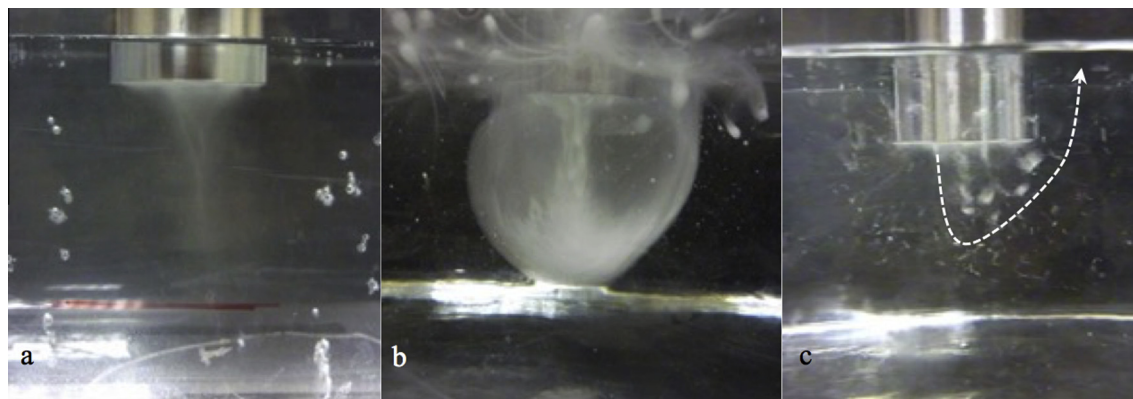
Fig. 2. Different cavitation bubble structures underneath the sonotrode tip forming a) a conical shape (water) and b) a circulating pattern with symmetrical vortexes (glycerine). In the case of the ethanol (c) bubbles are generated and dispersed outside the cavitation zone and towards the free surface as indicated by the white dashed arrow. Amplitude of the sonotrode tip (diameter 40 mm) was adjusted to its maximum, at 17 μm peak to peak.

Conical bubble structures, when formed, were stable and consisted of the acoustic streamers and interacting moving bubbles [18]; they can also be responsible for shielding and scattering effects that can drastically attenuate the ultrasonic propagation and the ultrasound field outside the conical bubble structure [23]. The mechanisms of conical bubble structure formation have been recently investigated by experimental observations [24] thus we will not dwell on this, but rather focus on spectral analysis features that will be discussed in Section 3.2.

3.1.2. Glycerine

Glycerine exhibited a distinct, slow development of the cavitation pattern below the sonotrode surface, making it a prime candidate for the observation of the mechanisms of cavitation inception and development of the cavitation zone in highly viscous environments. Unlike in water, an oscillating bubble in viscous glycerine does not easily break up into a cloud of small bubbles due to the suppressed jetting at high Re numbers while the effect of surface tension is considered to be negligible [25,26]. Damping of bubble oscillations by the viscosity of the liquid increases the oscillation period of the bubbles. The constriction of the bubble in the final stage of the collapse is lesser and most of the exerted energy is dissipated so that the bubble collapses less violently [27,28]. Consequently, there are fewer collapsing events. Due to the secondary Bjerknes forces that are responsible for bubble-bubble interactions [29], cavitation bubbles can attract or repel each other depending on the resonance frequency, their relative position, and the incident angle between the pressure node and the cavitating bubble [30].

At 50% power, bubbly streamers tended to move upwards (Fig. 3, curved dashed arrow at 19 s). Additionally, acoustic cavitation was observed at particular positions across and below the sonotrode surface as indicated by the arrows in Fig. 3 at 23 s as

well as in the areas where streamers migrate, i.e. near the bottom of the tank. There was no evidence for generation of cavitation events far away from the sonotrode surface. The cavitation pattern in glycerine was more confined than in water, with many micro bubbles accumulated around the sonotrode tip. Interestingly, the first bubbly streamer started its descending motion only after 23 s as can be seen from the dashed arrow in Fig 3. Thereafter, acoustic bursts from the tip face occasionally pushed existing bubbles further away from the acoustic horn. Once this "elastic shell" has broken, other bubbles could escape from the interior. After almost 85 s (Fig. 3), the number of bubbly streamers within the liquid volume became slightly larger and more consistent. However, the streamers were not stable enough to justify the formation of a developed cavitation environment. This implies that acoustic power was not adequate and buoyancy forces prevailed, allowing streamers to rest near the free surface as indicated by the arrow in Fig. 3 at 85 s. A more detail observation of the cavitation development in glycerine at 50% power can be found in the Supplementary material (Fig. 1s).

At 100% power, the bubbles underwent mutual attraction leading to the formation of bubble cluster 'grapes' (Fig 4, 0.6–1 s) similar to those previously reported in [30]. These cluster 'grapes' eventually led to the formation of stable bubbly structures similar to 'field lines' (see Fig. 2b and Fig 4). Favourable sites for further bubble growth were within those bubbly structures which behaved like 'elastic shells' and instead of growing spherically, they tended to form an elongated bubbly shape followed by a bubbly trail. These bubbly 'elastic shells' were then driven through the acoustic fluid streamers into the bulk liquid forming a broader and well-defined cavitation zone resembling an inverted mushroom (Fig. 4). A recirculating pattern started to develop in the time range 7–44 s (Fig. 4). The bubbly layers piled up with time, and soon a fully vortex-like structure was developed with a clear recirculating
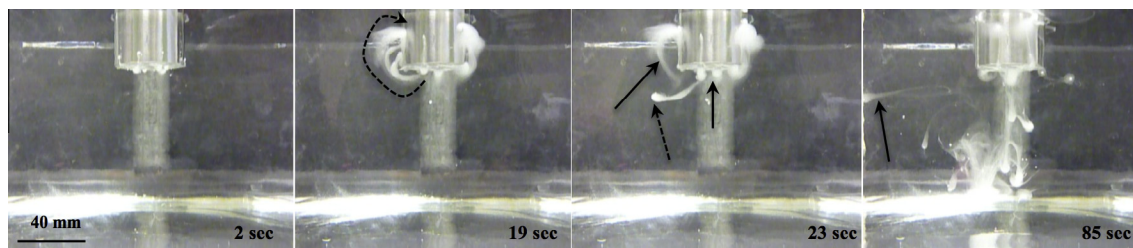

Fig. 3. Evolution of acoustic cavitation in glycerine solution. Amplitude of the sonotrode tip (diameter 40 mm) was adjusted at 50% (see also Fig. 1s in supplementary material).
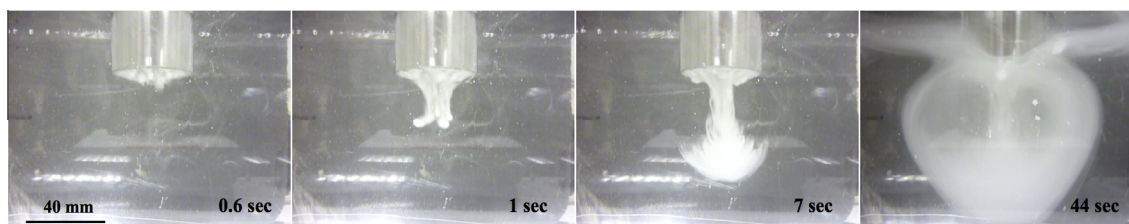
Fig. 4. Evolution of acoustic cavitation in glycerine solution. Amplitude of the sonotrode tip (diameter 40 mm) was adjusted to 100% (see also Fig. 2s in supplementary material).

pattern as the streamlines were going back into the main streamer. Additionally, the penetration depth also increased, reaching the bottom of the tank. The vortex slowly expanded with time while parts from the streamers escaped towards the free surface generating a haze-like pattern as shown in Fig. 4 after about 44 s. A more detail observation of the cavitation development in glycerine at 100% power can be found in the Supplementary material (Fig. 2s).

3.1.3. Ethanol

In liquid ethanol, for both given acoustic power values, neither streamer-like structures nor a stable cavitation zone were observed even when the cavitation regime had been established. Only fairly large individual cavitation bubbles (mm size) were visible. Specifically, in the case of 50% power (Fig. 5), inception of small cavitation bubbles was observed after 66 ms, forming plume structures which moved like clouds of smoke, the so-called 'smokers' [24]. 'Smokers' usually consist of many small bubbles appearing at the sonotrode tip surface. In this particular liquid, 'smokers' survived even further away from surfaces and inside the bulk liquid as can be seen from Fig. 5 after 66 ms and Fig. 6 after 33 ms (see dashed arrows). Then at about 396 ms (Fig. 5), the first large bubble appeared ($\approx$5 mm in diameter, see arrow) and subsequently more bubbles followed as can be seen after 528 ms. At this time, the cavitation regime was established, with large cavitation bubbles generated just below the sonotrode surface with a tendency of rapidly moving towards the free surface as shown in Fig. 2c while much smaller in size bubbles were distributed in the liquid bulk.

In contrast, when ultrasound with 100% power amplitude was applied to ethanol, cavitation bubbles moved initially towards the pressure antinodes one after another to form a structure, previously described as 'smokers' [24]. These 'smokers' then developed into the typical fractal branching pattern, the so-called Acoustic Lichtenberg Figures (ALF) [15] (see Fig. 6 after 99 ms). The series of frames in Fig. 6 shows the process of self-organization of bubbles into ALF formations in the pressure antinodes and then their disappearance, implying the change of the acoustic pressure regime in the bulk liquid and the transition to a more chaotic pressure field with bubbles forming, oscillating and floating randomly in the sonicated volume. Interestingly, in this power setting, large surviving bubbles (>5 mm) were absent

and a more homogeneous cavitation regime with many similar in size bubbles (in the range of a few hundred μm up to 2 mm) in a continuous motion and evenly distributed across the vessel was observed (Fig. 6 after 1980 ms). It seems, that bubbles were not pushed by the primary Bjerknes force towards the pressure nodes to form clusters or even if they were pushed they could easily escape and move towards the free surface due to their highly energetic 'wobbling' behaviour and large size (larger than the resonance radius) as has been previously shown in [31]. Coalescence of bubbles associated with the mutual attraction from the secondary Bjerknes forces was restricted (unlike the case of glycerine) alleviating their undisturbed motion into the liquid bulk. A more detail observation of the cavitation development in ethanol at 100% power can be found in the Supplementary material (Fig. 3s).

We observed that bubbles in ethanol grew rapidly, reaching a volume of several times their initial value, and remained in an oscillating pattern within the cavitation zone before gaining sufficient buoyancy to float to the surface (see Fig. 4s and video in Supplementary material). Rectified diffusion of vapour (cavitation bubbles grow or dissolve due to the mass transfer into/out of the bubbles) in fact governs the mechanism of growth and pulsation. As a result, large bubbles rapidly formed and could then easily float to the surface due to the buoyancy force instead of collapsing, a similar mechanism to that of ultrasonic degassing [2]. Results are in very good agreement with earlier work [31] where it was shown, using high-speed camera for a liquid with similar physical properties, that cavitation bubbles can indeed sustain their lifespan for many acoustic cycles due to the combination of surface and viscous forces in the liquid. Also relevant to these results is the work of Iwai and Li [32] where they reported that a lower surface tension in liquids significantly decreased the erosion rate due to the absence of major collapsing events and large bubble clusters. In terms of acquired velocity, bubbles in the case of 50% power had a slower ascent towards the free surface with an average speed of 0.18 ± 0.02 m/s (gained from the frame-by-frame analysis of the video sequence in Supplementary material) as compared to the bubbles in the case of 100% power where their average speed was measured to be around 0.25 ± 0.01 m/s (a typical cavitation bubble motion towards the free surface is shown in Fig. 5s in Supplementary material).
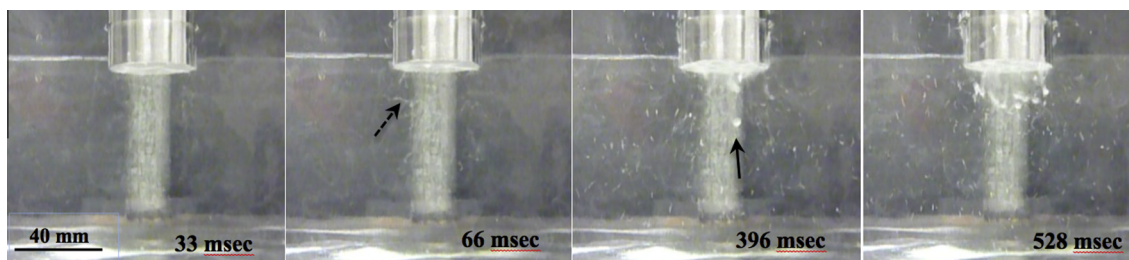

Fig. 5. Cavitation inception in liquid ethanol. Amplitude of the sonotrode tip (diameter 40 mm) was adjusted at 50%.
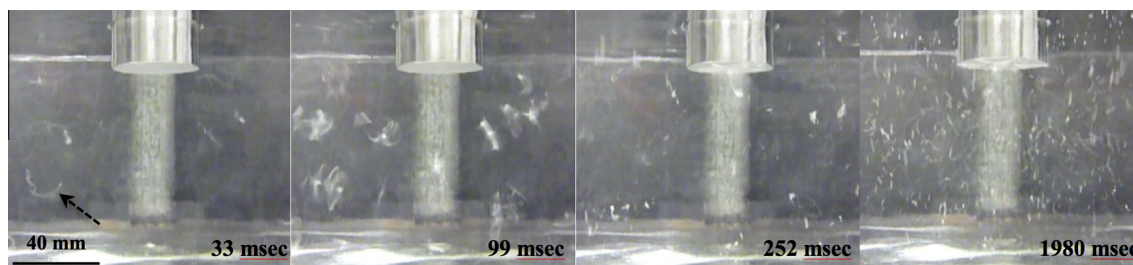
Fig. 6. Cavitation inception in liquid ethanol. Amplitude of the sonotrode tip (diameter 40 mm) was adjusted at 100% (see also Fig. 3s in supplementary material).

3.2. Spectrum analysis of the tested liquids

In the following sections, the spectra of the cavitation noise and acoustic emissions in the transparent three liquids are analysed. The level of acoustic noise is related to the acoustic pressure [6,12,13]. The frequency spectra in the ranges of 0–3 MHz and 0–10 MHz are shown in Figs. 7–10. The background noise is shown for reference only in Fig. 10. The background noise measurement was captured with the transducer switched off and the sonotrode submerged into the studied liquid and represents the own electrical excitation of the cavitometer electronics. Some discrete peaks found at MHz frequencies for all the liquids i.e. at 2, 2.3, and 4 MHz are solely related to the cavitometer as they appeared in all the spectra at those particular frequencies. The background noise level is very low compared to the levels of acoustic spectra (noting that the dBu scale is logarithmic) so this noise does not affect the levels and characteristics of the measured acoustic spectra.

3.2.1. Analysis of spectra up to 3 MHz
3.2.1.1. De-ionised water.
The highest amplitudes from cavitation emissions were recorded in de-ionised water. Interestingly, a higher measured cavitation activity was detected at the 50% power, and not at 100% at both cavitometer positions (Fig. 7). The ultrasonic wave propagation, and hence the pressure field distribution, is drastically altered by the presence of the conical bubble structure: the ultrasound field outside the conical bubble

structure is significantly weakened due to the shielding effect. A larger part of the sound energy is dissipated with the development of cavitation and a higher void (bubble) fraction below the ultrasound horn [33]. The increased number of cavitation bubbles absorb and scatter the sound waves, thereby weakening substantially the acoustic intensity away from the cavitation zone.

The 50% power experiment produced fewer visible bubbles than the 100% power, allowing the bubbles to migrate unimpeded by other bubbles, while their growth was smoother and their collapse was more symmetrical, producing a higher level of pressures. Similar and more distinguishable the results were obtained in the higher frequency domains of the spectra (MHz) (inset in Fig. 7 comparing lines '1' vs. '2' and '3' vs. '4') where the broadband noise increased systematically with the decrease in acoustic power, clearly supporting the shielding hypothesis.

3.2.1.2. Glycerine.
In this viscous liquid, the cavitation activity increased with power. Also, the intensity from the cavitation emissions was larger closer to the source (tip of the sonotrode). The broadband spectrum in Fig. 8 rose significantly with acoustic power from 50% to 100% implying that more transient cavitation was established. At the highest acoustic power, but at a distance from the cavitation zone, a periodic pattern was observed at higher frequencies, although not as distinctive as in ethanol (see below in Section 3.2.1.3 Ethanol). This is attributable to the acoustic emissions of linearly and non-linearly oscillating stable cavitation bubbles, with significant lifecycles (see also Section 2.4). Acoustic
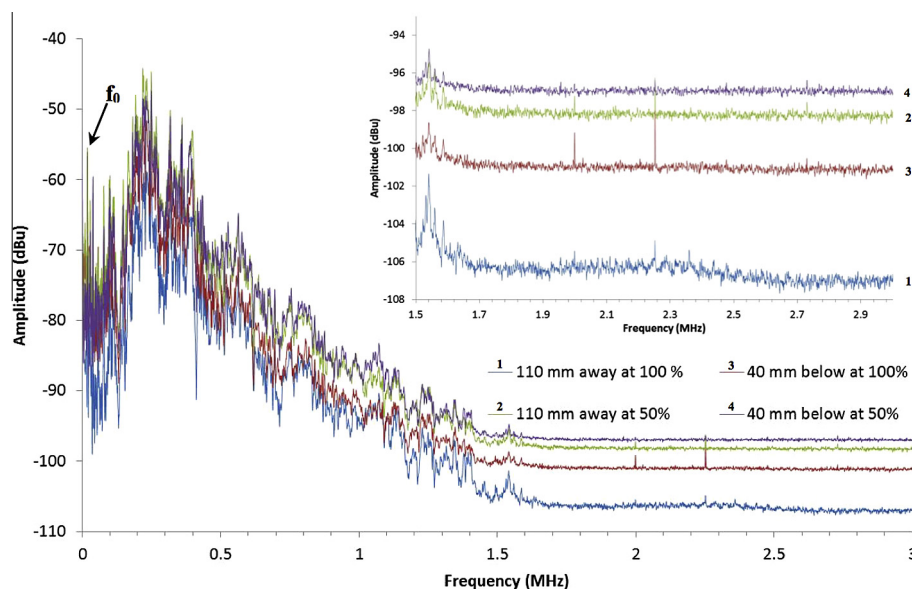

Fig. 7. Acoustic spectra in de-ionised water at different positions of the cavitometer (see Fig. 1) and different power settings of the transducer. Driving frequency (f_0) is 20 kHz.
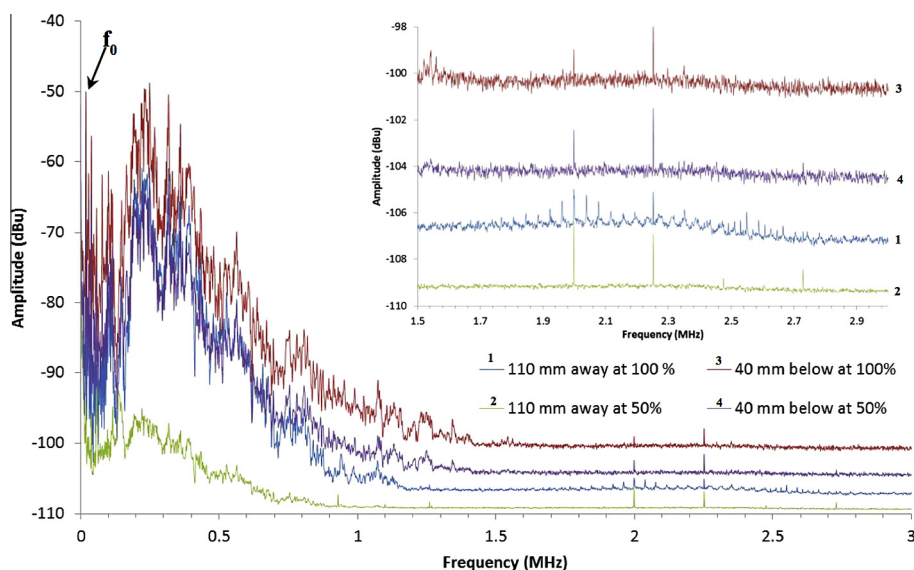
Fig. 8. Acoustic spectra in glycerine at different positions of the cavitometer (see Fig. 1) and different power settings of the transducer. Driving frequency (f_0) is 20 kHz.
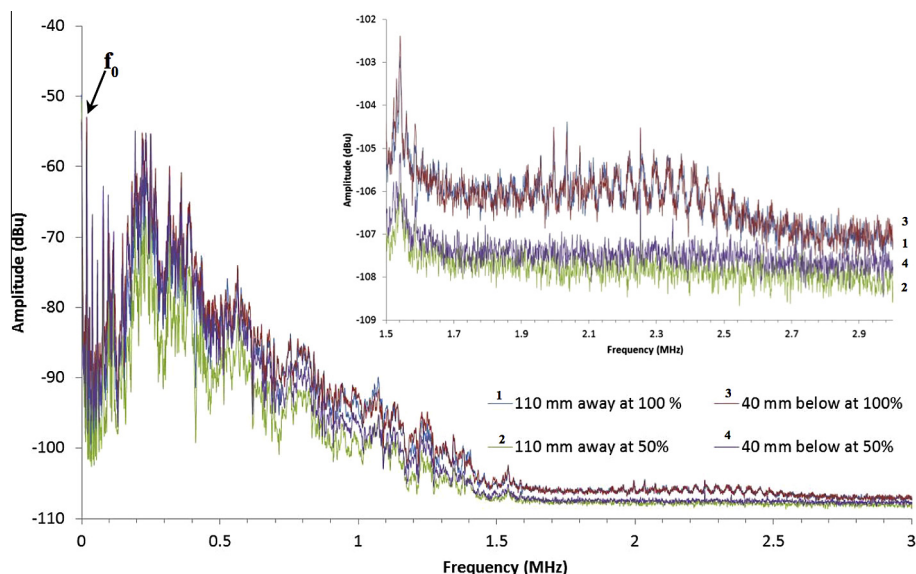

Fig. 9. Acoustic spectra in ethanol at different positions of the cavitometer (see Fig. 1) and different power settings of the transducer. Driving frequency (f_0) is 20 kHz.

emissions from these long-survived cavitation bubbles, mainly found away from the area of the cavitation zone, arrived to the probe undisturbed by the clusters of bubbles (as the probe was placed away from the cavitation zone). At the same time, the intensity of these emissions was rather small due to the damping from the highly viscous environment, generating consistent periodic patterns. At 50% power, the spectrum acquired at a distance of 110 mm from the source was very weak (intensity levels were close to that of the background noise level in Fig. 10) implying that acoustic emissions hardly arrived to the probe (low sound pressure), thus a very weak stable cavitation or no cavitation regime was generated in this location. These observations are in agreement with the work of Nomura et al. [34] where similar results were obtained in glycerine solutions using a hydrophone device, while erosion patterns on aluminium foil were negligible showing that the acoustic energy was greatly attenuated due to the high viscosity. In contrast, when the cavitometer probe was placed below the tip of the sonotrode inside the cavitation zone, transient

cavitation prevailed, increasing the broadband noise rather than forming the periodical patterns.

Comparing the results on acoustic spectra with the observations in Fig. 3, the shielding effect at the 50% power in glycerine was less pronounced than in water due to the less developed cavitation but the attenuation of acoustic signal was stronger due to the larger viscosity.

3.2.1.3. Ethanol. In the case of ethanol, peaks at in the lower frequency part of the spectrum (including the driving frequency and its harmonics) were sharper and more distinct compared with water and glycerine (Fig. 9). This correlated well with the observations that ethanol contained significantly more long-lived cavitation bubbles fluctuating in a stable linear or non-linear manner (see also Sections 2.4,3.1 and Fig. 4s and video in Supplementary material). This was due to the absence of bubbly cloud structures as shown in Figs. 5 and 6, so shielding and scattering effects did not significantly disturb the propagation of acoustic waves to
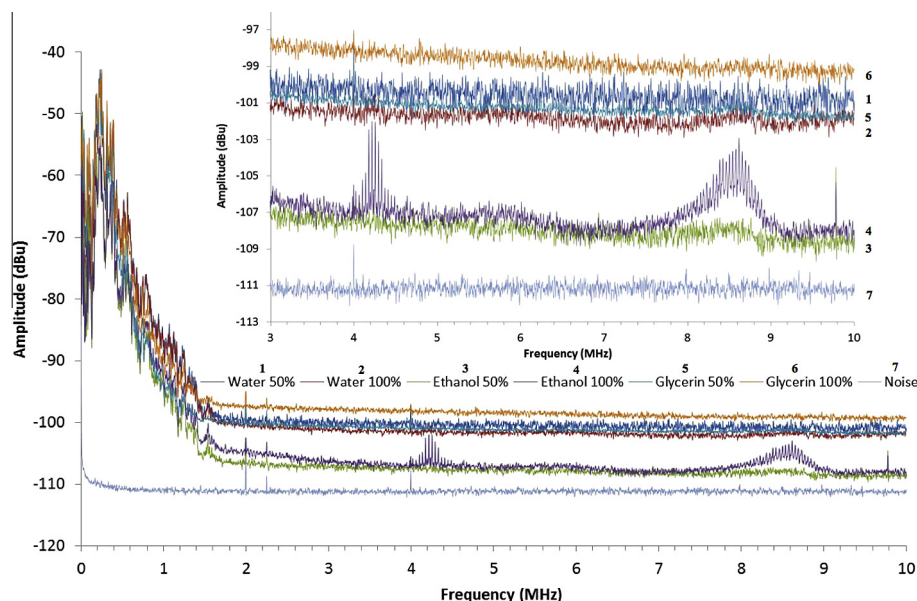
Fig. 10. Acoustic spectra determined up to a frequency range of 10 MHz for 3 different liquid environments at 2 different acoustic power levels: 1) water at 50%, 2) water at 100%, 3) ethanol at 50%, 4) ethanol at 100%, 5) glycerine at 50%, 6) glycerine at 100% and 7) background noise. Position of the cavitometer is below the sonotrode. Driving frequency (f_0) is 20 kHz.

longer distances and the formation of those high distinctive peaks testified for that. The large bubbles, i.e. mm size, contributed to the formation of the prominent peaks at low frequency. However, their acoustic emissions were not as powerful as in the other tested liquids, hence the overall spectrum had the weakest amplitude (dBu) values. Similar effects were reported in [23,35] where the erosive potential of similar organic liquids was investigated.

In ethanol, the spectrum in the high-frequency domain showed a periodic pattern with prominent peaks (see inset in Fig. 9), rather than being non-linear and chaotic as expected from shock waves and other non-linear contributions in transient cavitation. The hypothesis is that, in addition to larger bubbles, many tiny long-lived bubbles 2–3 μm in size estimated according to the Minnaert equation [36] (which could not be optically resolved in our experiments) were generated and stably oscillated, giving rise to the observed well-defined structures at MHz frequencies (see also Section 2.4). Periodic features of the spectrum at MHz frequencies (see inset in Fig. 11) suggest that many cavitation bubbles vibrated in phase and this number was much greater than in water and glycerine. This may be explained by the large ethanol vapour pressure (5.3 kPa at 20 °C) compared with those of water and glycerine (see Table 1). Note that the bubbles in ethanol were frequently observed being captured in what appears to be the pressure nodes of standing waves especially in the downstream of the cavitation zone (see Fig. 6). Bubbles remained there pulsating for a significant period of time before they eventually moved to the upper surface. Evidence of bubble oscillations around the same location and their migration towards the free boundary can be seen in the video available in Supplementary material. The number of bubbles captured at the pressure nodes of the standing waves was significant as compared to the other two fluids, suggesting further contributions from these long-lived pulsating cavitation bubbles to the acoustic spectrum.

Distinguishable MHz-frequency periodic patterns were only observed at 100% where the acoustic power was sufficient to generate a significant number of smaller in size cavitation bubbles (as discussed in Section 3.1 and shown in Fig. 6).

Broadband noise levels in ethanol were much less affected by the distance from the sonicated source irrespective of the level of power. The acoustic intensity was measured to be at the same levels everywhere in the liquid bulk, suggesting that in ethanol the distance from the source did not play so decisive role like in glycerine. The assumption is that stable linear and non-linear cavitation prevailed over transient behaviour; so instead of a substantial rise of the broadband noise with the increased ultrasonic power, we observed periodicity resulting from i) in-phase vibration of numerous cavitation bubbles in the liquid; ii) multiple reflections where signals of similar frequencies are combined and iii) undisturbed propagation of acoustic waves in the bulk due to the absence of significant bubbly clusters and, hence, shielding [15].

As both power levels (50% and 100%) produced similar cavitation intensity in the low-frequency range of the acoustic spectrum, cavitation in this environment could be considered well developed irrespective of the tested power amplitude.

These experiments demonstrated the importance of vapour pressure as well as the surface tension and the viscosity of the liquid for cavitation development, which is in a good agreement with Ref. [37]. For example, liquids like ethanol, with larger vapour pressure or smaller surface tension than water will exhibit lower cavitation noise level compared to water. If liquid viscosity is significantly increased, i.e. from 1 to 1500 cSt, as in the case of the glycerine (see Table 1), the level of cavitation noise tends to increase. Thus, it can be clearly seen that cavitation intensity can be treated as a physical quantity/parameter which is related to the combination of many different physical parameters found in a liquid and it can be used for characterizing physical properties of liquids.

3.2.2. Spectral analysis up to 10 MHz

Fig. 10 shows acoustic spectra in a higher MHz range for all the tested transparent liquids obtained using the cavitometer probe placed below the tip of the sonotrode. It is apparent from the corresponding spectrograms that glycerine at 100% power had the highest broadband cavitation noise closely followed by water at 50% then glycerine at 50% and water at 100%. The reasons for this were discussed in the previous section.

Here we would like to focus on some special features of the ethanol spectra. Broadband cavitation noise was much weaker in
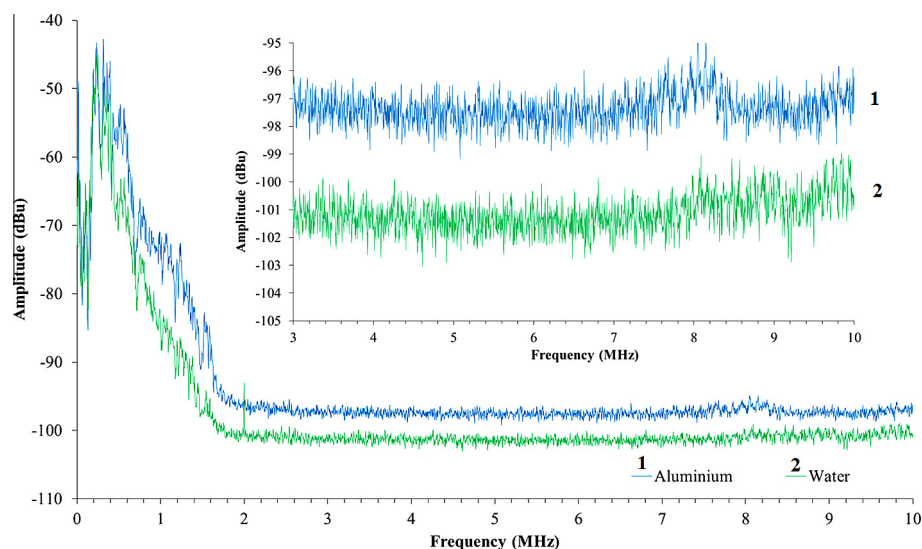
Fig. 11. Acoustic spectra generated by magnetostrictive ultrasonic transducer at 17.5 kHz driving frequency (f_0) and measured with the cavitometer tip positioned about 3–4 cm below the sonotrode's tip in (a) water and (b) liquid Al. Inset shows the spectrum in the range of up to 10 MHz.

the case of the ethanol (about 10 times lower than the maximum cavitation intensity measured in glycerine) but distinctive peaks appeared in the spectrum at frequencies of 4–4.5 MHz and 8–9 MHz when the transducer power is at 100% (see inset in Fig. 10, line 4). The presence of these high intensity peaks in the high frequency domain of the spectra can be correlated with linear pulsations of tiny bubbles around 1–1.5 μm in size (according to Minnaert equation [36]) for this particular setup. This is in good agreement with the series of experiments performed by Jomni et al. [38] where they showed that small bubbles (of the order of 1 μm) stay spherical throughout their lifetimes. The reason that these acoustic spectrum features were not observed in ethanol at 50% (line 3 in the inset in Fig. 10) is possibly because this power was not sufficient to form enough small bubbles vibrating in phase. This is supported by the visual observations presented in Section 3.1, where only at 100% power (Fig. 6) bubbles were uniformly distributed in smaller and in similar sizes within the liquid bulk of ethanol, implying that the chances for a number of bubbles to vibrate in phase giving rise to the formation of such distinct acoustic spectrum features were significant.

3.3. Dimensionless analysis of the tested liquids and the choice of a transparent analogue for cavitation studies in liquid aluminium

Ultrasonic melt processing is known to significantly improve the properties and quality of metallic materials, e.g. aluminium alloys [2]. Due to difficulties in processing large volumes of melt,

this technology has not been yet transferred to industry. A fundamental understanding of the cavitation efficiency of ultrasonic treatment is required to circumvent these difficulties. The opacity of aluminium melts limits the direct studies of cavitation processing to the measurements of acoustic noise within the bulk and X-ray radiography of small samples. The former technique was until recently mostly qualitative [2] and the latter just reached enough maturity to produce some valuable results yet remaining complicated and limited to very small volumes [11,39]. The motivated choice of a transparent analogue that can be used for the assessment of cavitation processes in liquid aluminium (and potentially other liquid metals) is very important.

To compare the material properties of the liquids under investigation between themselves and with liquid aluminium, the relevant dimensionless quantities are computed, as listed in Table 2. Bond and Prandtl number are the non-dimensional quantities that depend on material properties while other numbers depend on the flow [40] (see Appendix A for formulations).

Water and aluminium share the closest flow properties as shown by their close Reynolds numbers (Re) in Table 2. In this table, the macroscopic Re corresponds to the macroscopic flow below the sonotrode (with the reference length chosen as the diameter of the sonotrode: 40 mm). The microscopic Re corresponds to flow around a bubble, with the reference length chosen as the resonant diameter of the bubble at 20 kHz. The small Ohnesorge numbers in aluminium and water show that the ratio of the viscous to the inertial and surface tension forces is similar

Table 2
Comparison between the calculated properties and dimensionless quantities for water, glycerine, ethanol, and liquid aluminium for similar flow velocities. The reference velocity V is equal to 0.1 m/s, typical flow velocity in acoustic flow and in melt transport systems. For the microscopic Re, the reference length L is equal to the resonant diameter of the bubble at 20 kHz, calculated from the Minnaert relationship [36]. For the macroscopic Re, the reference length is the diameter of the sonotrode.

	Water	Glycerine	Ethanol	Aluminium
Temperature (°C)	20	20	20	700
Sound wavelength λ at 20 kHz (mm)	74.1	100	55	230
Absorption coefficient α/f^2, $\times 10^{15}$ (Np s^2 m^{-1})	8.1	2500	28	0.18
Resonant bubble diameter L (μm)	138.2	131.8	145.6	117.3
Bond number (Bo), $\times 10^4$	23.7	33.5	74.2	3.7
Prandtl number (Pr)	7.2	8.1×10^3	1.9×10^2	3.6×10^{-3}
Microscopic Reynolds number (Re)	13.8	1.75×10^{-2}	10.4	27.9
Macroscopic Reynolds number (Re)	4000	5.3	2854.5	9500
Ohnesorge number (Oh)	9.6×10^{-3}	9.2	2.2×10^{-2}	2.0×10^{-3}
Weber number (We)	1.7×10^{-2}	2.6×10^{-2}	5.2×10^{-2}	3.2×10^{-3}

in both liquids and very small if compared with glycerine: the influence of viscosity in both fluids is expected to be minimal.

The ratio of surface tension forces compared to body forces is high for all fluids: high surface tension should help in maintaining the spherical shape of the bubbles as they move in the liquid bulk. The Weber number is smallest for aluminium, suggesting that bubbles in aluminium are very stable and spherical. This is in agreement with our recent observations performed in the National Sychrotron facility in UK where X-ray radiographs show that cavitation bubbles sustain stable spherical behaviour [39]. Ethanol bubbles with the largest Weber number are more prone to instabilities, as also discussed in Section 3.1.

Thermal diffusion in the case of ultrasonic wave propagation results from temperature gradient between regions of compression and expansion. The compression in a fluid produces a local increase in temperature, while the neighbouring layers which is in a state of rarefaction cool down. Consequently heat flows from the compressed layers to the rarefied layers and thus a portion of energy is converted to heat. In liquid aluminium heat conductivity would be the dominant heat transfer process over convection as shown by its low Prandtl number, and the attenuation of the acoustic waves propagation (sound converts to heat) in this medium is significant. In the tested non-metallic liquids that are good heat insulators, convection will be the dominant mechanism for heat dissipation.

In ethanol, the distance from the acoustic source does not affect much the propagation of the acoustic waves (Fig. 10), while in liquid aluminium the acoustic pressure is strongly affected by the distance from the source [41]. Thus ethanol could not be considered as a suitable analogue of liquid aluminium.

In contrast to ethanol, glycerine and water share a similar structure in their acoustic spectra as shown in Fig. 10, however the developed cavitation zone is significantly different in these liquids as is evident from Fig. 2. Recently, *in situ* high-speed synchrotron studies showed that water and liquid aluminium have very similar geometry of the developed cavitation zone just below the tip of the sonotrode [42,43]. Additionally, latest studies showed that the general shape and main features of the acoustic spectrum in liquid aluminium is comparable to that of the water with differences observed in the intensity of the acoustic emissions [13]. Also, with the increment of the power from the acoustic source (i.e. from 50% to 100%) water and aluminium demonstrate similar shielding behaviour (as explained in Section 3.2.1 for de-ionised water and seen for liquid aluminium in [41]), unlike the case of glycerine where cavitation intensity increases with power. Thus, it is apparent that liquid aluminium in terms of cavitation development and behaviour is closer related to water than to other tested liquids.

To confirm this similarity, a comparison of acoustic spectra in water and liquid aluminium over a wide range of frequencies was performed in this study. Fig. 11 demonstrates that the spectra for both of the tested liquids follows a similar pattern across the whole broadband spectrum reinforcing further the opinion that water and liquid aluminium share similar behaviour under ultrasonic treatment. In the case of cavitation intensity, the main difference is that the broadband spectrum is significantly higher in the case of liquid aluminium as compared with water, the reasons for that are discussed elsewhere [13]. Particularly, in the spectrum domain up to 2 MHz, broadband noise is 10–20 dBu on average higher in aluminium than for water while for the region above 2 MHz and up to 10 MHz (associated solely with cavitation emissions from the collapse of bubbles) this difference drops to approximately 4 dBu on average, still showing the greater dynamics of cavitation bubbles in liquid aluminium. This also implies that transient cavitation associated with the level of the broadband cavitation noise is generally more prominent in liquid aluminium and thus higher activity from the cavitation bubbles is expected.

Note that the background noise level in these experiments was similar to that shown in Fig. 10.

Despite the physical evidence that water and liquid aluminium are quite similar in cavitation behaviour, the comparison of the non-dimensional numbers (Table 2) suggests that none of the tested liquids resembles perfectly liquid aluminium, with water just being the closest possible candidate. The approach taken in this study can be nevertheless used for further search of a transparent analogue closest to the features of liquid metals, by selecting a proper combination of physical properties such as viscosity, density and surface tension, e.g. through mixing of different liquids.

4. Concluding remarks

Cavitation noise spectra carry a multitude of information in their respective ultra-harmonic and broadband components as has been clearly exhibited by the results presented in this paper. This can help to a) distinguish different regimes of acoustic cavitation, such as stable cavitation and inertial cavitation, b) quantify the cavitation activity/events and determine their intensity, c) determine the regions of higher cavitation activity where prominent peaks prevail, d) estimate the resonant size of the cavitation bubbles from sharp distinctive peaks in the spectrum, e) better understand the relation of cavitation activity with various liquid properties, which can be the key for a general theory behind the development of cavitation in any liquid type, including liquid metals.

In this paper, three liquids with significantly different physical properties were investigated under continuous sonication at different acoustic power levels. Results showed that their behaviour is very different because their physical parameters, i.e., vapour pressure, surface tension, viscosity etc. play a decisive role in the establishment of the cavitation regime. Key findings of the study are:

- The formation of a cavitation zone in water (conical bubble structure) and in glycerine (thick round layer) is apparent. In ethanol, even at the highest amplitude of the transducer at 100% power, bubbles are dispersed and vigorously oscillate towards the free surface (similar as in ultrasonic degassing) rather than creating complicated bubbly structures and multiple collapsing events.
- The main feature of glycerine at 50% power is the confining "shell" of cavitation zone around the horn tip. It is frequently penetrated by spurious jets allowing other bubbles to escape. In contrast, at 100% power a continuous bubbly streamer is established revealing the boundaries of the cavitation zone (resembling an inverted mushroom) with the increased overall cavitation activity.
- In general, cavitation intensity levels in water and glycerine are of a similar dBu range and considerably higher than in ethanol.
- Distinctive peaks at high-frequency are observed in the case of ethanol solution at 100% power. These emissions can reflect the stable non-linear or linear oscillation of bubbles of μm size. Distance from the acoustic source does not affect the propagation of the acoustic waves in ethanol.
- Water shares the closest cavitation properties with liquid aluminium as indicated by the spectra analysis and their calculated dimensionless quantities and is therefore the most appropriate liquid among those tested to replicate liquid aluminium. There is a potential to use the cavitometer measurements to design transparent liquid mixtures that would match liquid metals more closely.
- In a technological context, cavitation noise (MHz) can serve as a metrological tool for cavitation activity in industrial systems of various scales where direct (optical) observation and analysis is not possible. The fact that cavitation noise spectra carry a multitude of information in their respective ultra-harmonic

and broadband components can help in distinguishing different regimes of acoustic cavitation. With extensive knowledge of cavitation behaviour at different liquid environments, extrapolation to high temperature and opaque liquid melts like aluminium can be achieved.

Acknowledgements

Appendix A.

Dimensionless numbers used in this study
Bond number

$$Bo = \frac{\rho g L^2}{\sigma}$$

Prandtl number

$$Pr = \frac{\mu c_p}{\kappa}$$

Reynolds number

$$Re = \frac{\rho V L}{\mu}$$

Ohnesorge number

$$Oh = \frac{\mu}{\sqrt{\rho \sigma L}}$$

Weber number

$$We = \frac{\rho V^2 L}{\sigma}$$

Nomenclature

ρ (kg/m^3)	Density
g (m/s^2)	Gravitational acceleration
L (m)	Characteristic length
σ (N/m)	Surface tension
μ (Pa s)	Dynamic viscosity
c_p (J/kg K)	Specific heat
κ (W/m K)	Thermal conductivity
V (m/s)	Maximum bubble velocity

Appendix B. Supplementary data

Supplementary data associated with this article can be found, in the online version, at http://dx.doi.org/10.1016/j.ultsonch.2016.06.034.

References

[1] V.I. Il'ichev, In Proc. Akustichesky Institut Akademii Nauk SSSR (AKIN) 6, 1969, pp. 16–29.
[2] G.I. Eskin, D.G. Eskin, Ultrasonic treatment of light alloy melts, second ed., Series: Advances in Metallic Alloys, CRC Press, Boca Raton, 2014.
[3] I. Tzanakis, D.G. Eskin, A. Georgoulas, D. Fytanidis, Incubation pit analysis and calculation of the hydrodynamic impact pressure from the implosion of an acoustic cavitation bubble, Ultrason. Sonochem. 21 (2014) 866–878.
[4] I. Tzanakis, W.W. Xu, D.G. Eskin, P.D. Lee, N. Kotsovinos, In situ observation and analysis of ultrasonic capillary effect in molten aluminium, Ultrason. Sonochem. 27 (2015) 72–80.
[5] M. Hauptmann, H. Struyf, P. Mertens, M. Heyns, S. De Gendt, C. Glorieux, S. Brems, Towards an understanding and control of cavitation activity in 1 MHz ultrasound fields, Ultrason. Sonochem. 20 (2013) 77–88.
[6] I. Tzanakis, M. Hodnett, G.S.B. Lebon, N. Dezhkunov, D.G. Eskin, Calibration and performance assessment of an innovative high-temperature cavitometer, Sens. Actuators A 240 (2016) 57–69.
[7] B. Zeqiri, P.N. Gelat, M. Hodnett, N.D. Lee, A novel sensor for monitoring acoustic cavitation, Part I: concept, theory and prototype development, IEEE Trans. Ultrason. Ferroelectr. Freq. Control 50 (10) (2003) 1342–1350.
[8] E.A. Neppiras, Subharmonic and other low-frequency signals from sound-irradiated liquids, J. Sound Vib. 10 (1969) 176–180.
[9] M. Hodnett, R. Chow, B. Zeqiri, High-frequency acoustic emissions generated by a 20 kHz sonochemical horn processor detected using a novel broadband acoustic sensor: a preliminary study, Ultrason. Sonochem. 11 (2004) 441–454.
[10] T.J. Mason, A.J. Cobley, J.E. Graves, D. Morgan, New evidence for the inverse dependence of mechanical and chemical effects on the frequency of ultrasound, Ultrason. Sonochem. 18 (2011) 226–230.
[11] I. Tzanakis, W.W. Xu, G.S.B. Lebon, D.G. Eskin, K. Pericleous, P.D. Lee, In situ synchrotron radiography and spectrum analysis of transient cavitation bubbles in molten aluminium alloy, Phys. Procedia 70 (2015) 841–845.
[12] D.G. Eskin, K. Al-Helal, I. Tzanakis, Application of a plate sonotrode to ultrasonic degassing of aluminium melt, J. Mater. Process. Technol. 222 (2015) 148–154.
[13] I. Tzanakis, G.S.B. Lebon, D.G. Eskin, K.A. Pericleous, Characterisation of the ultrasonic acoustic spectrum and pressure field in aluminium melt with an advanced cavitometer, J. Mater. Process. Technol. 229 (2016) 582–586.
[14] G.J. Speight, Lange's Handbook of Chemistry, McGraw-Hill, New York, 2005.
[15] T.G. Leighton, The Acoustic Bubble, Academic Press, London, 1994.
[16] J. Eisener, J. Schneider, C. Cairós, R. Mettin, Sound films of acoustic cavitation, in: AIA-DAGA 2013, Proceedings of the International Conference on Acoustics 2013, Merano, Deutsche Gesellschaft für Akustik e.V. (DEGA), Berlin, 2013, pp. 485–488.
[17] A. Znidarcic, R. Mettin, M. Dular, Modeling cavitation in a rapidly changing pressure field – application to a small ultrasonic horn, Ultrason. Sonochem. 22 (2015) 482–492.
[18] A. Moussatov, C. Granger, B. Dubus, Cone-like bubble formation in ultrasonic cavitation field, Ultrason. Sonochem. 10 (2003) 191–195.
[19] V.N. Skokov, A.V. Reshetnikov, A.V. Vinogradov, V.P. Koverda, Fluctuation dynamics and 1/f spectra characterizing the acoustic cavitation of liquids, Acoust. Phys. 53 (2) (2007) 136–140.
[20] V.N. Skokov, V.P. Koverda, A.V. Reshetnikov, A.V. Vinogradov, 1/f fluctuations under acoustic cavitation of liquids, Phys. A 364 (2006) 63–69.
[21] N.V. Malykh, G.N. Sankin, Stabilization and acoustic spectra of a cavitation cluster in an ultrasonic spherical cavity, Tech. Phys. 55 (2010) 92–97.
[22] M. Plesset, Cavitation erosion in non-aqueous liquids, ASME J. Basic Eng. 92 (1970) 807–813.
[23] M.M. van Iersel, N.E. Benes, J.T.F. Keurentjes, Importance of acoustic shielding in sonochemistry, Ultrason. Sonochem. 15 (2007) 294–300.
[24] L. Bai, W. Xu, J. Deng, C. Li, D. Xu, Y. Gao, Generation and control of acoustic cavitation structure, Ultrason. Sonochem. 21 (2014) 1696–1706.
[25] B. Karri, K. Pillai, E. Klaseboer, S. Ohl, B. Khoo, Collapsing bubble induced pumping in a viscous fluid, Sens. Actuators A 169 (2011) 151–163.
[26] S. Popinet, S. Zaleski, Bubble collapse near a solid boundary: a numerical study of the influence of viscosity, J. Fluid Mech. 464 (2002) 137–163.
[27] X.M. Liu, X. H. Liu, J. He, Y. Hu, J. Lu, X. Ni, Cavitation bubble dynamics in liquids of different viscosity, in: Symposium of Photonics and Optoelectronic, SOPO 2010-Proceedings 5504305, 2010.
[28] N. Pelekasi, A. Gaki, A. Doinikov, J. Tsamopoulos, Secondary Bjerknes forces between two bubbles and the phenomenon of acoustic streamers, J. Fluid Mech. 500 (2004) 313–347.
[29] S. Sepehrirahnama, K.M. Lim, F.S. Chau, Numerical study of interparticle radiation force acting on rigid spheres in a standing wave, J. Acoust. Soc. Am. 137 (2015) 2614–2622.
[30] A.A. Doinikov, Bubble and Particle Dynamics in Acoustic Fields: Modern Trends and Applications, Research Signpost, Kerala, 2005, pp. 95–143.
[31] I. Tzanakis, M. Hadfield, I. Henshaw, Observations of acoustically generated cavitation bubbles within typical fluids applied to a scroll expander lubrication system, Exp. Thermal Fluid Sci. 35 (2011) 1544–1554.
[32] Y. Iwai, S. Li, Cavitation erosion in waters having different surface tensions, Wear 254 (2003) 1–9.
[33] L.D. Rozenberg, Powerful ultrasonic fields, Part VI Cavitation Region, 171, Nauka, Moscow, 1968, pp. 221–266.
[34] S. Nomura, K. Murakami, Y. Sasaki, Streaming induced by ultrasonic vibration in a water vessel, Jpn. J. Appl. Phys. 39 (2000) 3636–3640.
[35] I. Tzanakis, N. Garland, M. Hadfield, Cavitation damage incubation with typical fluids applied to a scroll expander system, Tribol. Int. 44 (12) (2011) 1668–1678.
[36] M. Minnaert, On musical air bubbles and the sound of running water, Philos. Mag. 16 (1933) 235–248.
[37] O.V. Abramov, V.O. Abramov, M.S. Mullakaev, V.V. Artem'ev, The Efficiency of ultrasonic oscillations transfer into the load, Acoust. Phys. 55 (2009) 894–909.
[38] F. Jomni, F. Aitken, A. Denat, Dynamics of microscopic bubbles generated by a corona discharge in insulating liquids: influence of pressure, J. Electrostat. 47 (1999) 49–59.

[39] W.W. Xu, I. Tzanakis, P. Srirangam, S. Terzi, W. Mirihanage, D.G. Eskin, A.J. Bodey, P. Lee, Synchrotron quantification of ultrasound cavitation and bubble dynamics in Al–10Cu melts, Ultrason. Sonochem. 31 (2016) 355–361.

[40] B.R. Munson, A.P. Rothmayer, T.H. Okiishi, W.W. Huebsch, Fundamentals of Fluid Mechanics, seventh ed., John Wiley & Sons, Hoboken, 2013.

[41] I. Tzanakis, G.S.B. Lebon, D.G. Eskin, K.A. Pericleous, Investigation of the factors influencing cavitation intensity during the ultrasonic treatment of molten aluminium, Mater. Des. 90 (2016) 979–983.

[42] H. Huang, D. Shu, J. Zeng, F. Bian, Y. Fu, J. Wang, B. Sun, In situ small angle X-ray scattering investigation of ultrasound induced nucleation in a metallic alloy melt, Scripta Mater. 106 (2015) 21–25.

[43] D. Tan, T.L. Le, J.C. Khong, T. Connolley, K. Fezza, J. Mi, High-speed synchrotron X-ray imaging studies of the ultrasound shockwave and enhanced flow during metal solidification processes, Metal. Mater. Trans. A 46A (2015) 2851–2861.